DOA estimation of two targets using beamformer based methods with application to automotive radar

Richtungsschätzung von zwei Zielen mit Beamformer-basiererten Verfahren und Kfz-Radar Anwendung

Master-Thesis von Javier Cordero

14. September 2011

TECHNISCHE UNIVERSITÄT DARMSTADT

DOA estimation of two targets using beamformer based methods with application to automotive radar
Richtungsschätzung von zwei Zielen mit Beamformer-basiererten Verfahren und Kfz-Radar Anwendung

Vorgelegte Master-Thesis von Javier Cordero

1. Gutachten: Dipl.-Ing. Philipp Heidenreich
2. Gutachten: Prof. Dr.-Ing. A. Zoubir

Tag der Einreichung:

Declaration / Erklärung

To the best of my knowledge and belief this work was prepared without aid from any other sources except where indicated. Any reference to material previously published by any other person has been duly acknowledged. This work contains no material which has been submitted or accepted for the award of any other degree in any institution.

Hiermit versichere ich die vorliegende Arbeit ohne Hilfe Dritter nur mit den angegebenen Quellen und Hilfsmitteln angefertigt zu haben. Alle Stellen, die aus Quellen entnommen wurden, sind als solche kenntlich gemacht. Diese Arbeit hat in gleicher oder ähn licher Form noch keiner Prüfungsbehörde vorgelegen.

Darmstadt, den 14. September 2011

_____

(Javier Cordero)

Abstract

Direction-of-arrival (DOA) estimation of two targets plays an important role in automotive radar. Two cases are distinguished: when the targets are closely spaced and the conventional beamformer is not able to resolve them, and when the targets are widely spaced and the beamformer is able to resolve them.

In the first case, accurate estimates can be obtained using high-resolution techniques. In the second case, estimates are typically biased. Automotive radar applications demand real-time processing and therefore the computational cost has to be addressed. For the resolved scenario, we propose a procedure to reduce the bias of the beamformer estimates, thus avoiding the use of iterative algorithms. The final estimates are obtained after applying a correction term, which is calculated off-line and stored in a look-up table.

For the non-resolved scenario, we consider a practicable implementation of the maximum likelihood estimator. A simplified version of the cost function is used to reduce the complexity. The peak location from the beamformer can also be used to delimit the search range.

The results of the mentioned methods are compared with other iterative algorithms, in terms of performance and computational cost. Applying the correction factors, the bias of the beamformer estimates are successfully reduced, making them accurate enough for the automotive radar application. The simplified implementation of the ML cost function reduces significantly the computational cost, allowing its use in real-time applications. Moreover, the performance obtained is also within the acceptable range for the automotive radar application, even for narrow angular separations. A block diagram containing the proposed methods is finally given, which is proposed as a suitable DOA estimation system for the automotive radar application.

Abbreviations, Acronyms and Symbols

ACC	adaptative cruise control
ADAS	advanced driver assistant system
ANP	alternating notch periodogram
AP	alternating projection
AWGN	additive white Gaussian noise
BF	beamformer
BW	beamwidth
CRB	Cramer-Rao bound
DOA	direction of arrival
FFT	fast Fourier transform
GS	global search
LCA	lane change assistant
LUT	look-up table
MC	Monte-Carlo
MLE	maximum likelihood estimation
RMSE	root mean squared error
SNR	signal-to-noise ratio
ULA	uniform linear array
$(\cdot)^{\dagger}$	the pseudoinverse
$\hat{\theta}$	estimate or estimator of a parameter θ
σ^2	variance

Contents

1 Introduction

In today's passenger vehicles, sophisticated security applications can be offered by using the radar technology. Some examples of advanced driver assistant systems (ADAS) based on radar applications are: adaptive cruise control (ACC), forward collision warning (FCW) or lane change assistant (LCA). In all of them, a sequence of radar pulses is used to illuminate the scene, and the information of the vehicle environment is obtained by analyzing the data collected from a receiving antenna array. The classification of surrounding targets is possible by applying radar pre-processing, which divides the received data into processing cells, corresponding to range and relative velocity. Each processing cell contains a single snapshot [6]. Direction-of-arrival (DOA) estimation for a single target can be optimally solved by using the conventional beamformer (BF), which is the maximum likelihood estimator (MLE) for this scenario [3].

Nevertheless, the two-target case is also present in the automotive radar application, which typically occurs when a ghost target is introduced in the system due to specular multipath with the guardrail, as illustrated in the figure below.

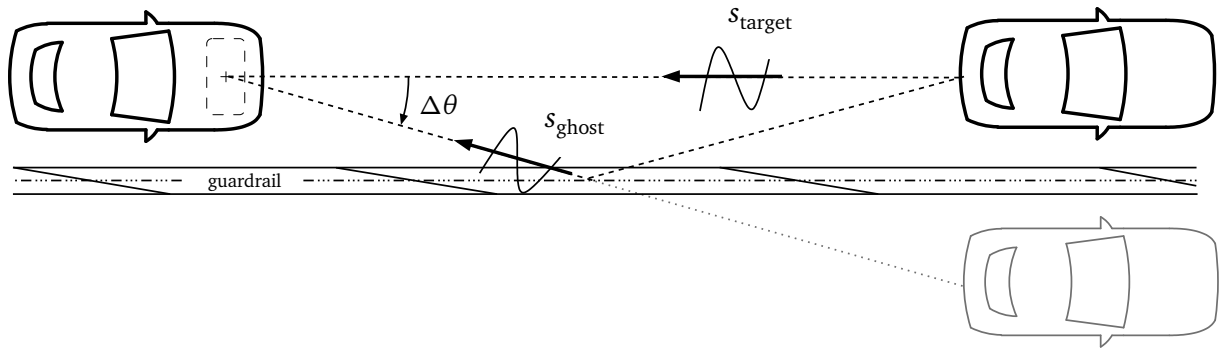

Figure 1.1: Two-target scenario with specular multipath with the guardrail.

In these situations, the BF method may not be able to resolve closely spaced targets. If it is able to resolve the targets, it typically produces biased estimates.

In the resolved case, other iterative techniques can be used to obtain more accurate estimates, such as the RELAX algorithm [4], the method of alternating projections (AP) [13] or the alternating notch periodogram (ANP) algorithm [2]. All mentioned MLE implementations divide the two-target problem into a sequence of single-target problems, requiring a few iterations to reach the corresponding convergence conditions.

Referring to the non-resolved case, the iterative techniques may require many iterations when the targets are closely separated, and moreover their iterative nature makes them difficult to parallelize.
Subspace-based methods are also commonly presented as a high-resolution alternative for DOA estimation, e.g. the MUSIC algorithm [7]. However, we do not consider them as a possible solution for the scenario in this thesis, for two reasons:

- On the one hand, subspace-based methods require an eigendecomposition of the spatial covariance matrix, which is computationally complex and also hard to parallelize.
- On the other hand, the estimation for closely spaced targets fails when a low number of snapshots are used, and particularly for highly correlated signals [3].

In contrast to subspace-based methods, the MLE is statistically efficient for two correlated targets in the non-resolved case, and still when a single snapshot is available [10]. Nevertheless, a direct implementation of the MLE requires a two-dimensional search, in which a computationally complex cost function has to be evaluated at each grid point. Therefore, the computational burden is again the main drawback.

In this document, we present fast procedures for estimating the DOA parameters in both the resolved and the non-resolved case. We first consider an initial estimation by using the BF method. Depending on the situation, this is followed by:

a) Resolved scenario:

   We identify this case by the presence of two main beams in the BF spectrum. The estimated parameters are obtained after applying a bias correction term, which is calculated off-line and stored in a look-up table (LUT).

b) Non-resolved scenario:

   In this case, only a single main beam is present in the BF spectrum, which corresponds to the superposition of both targets. The BF peak location is used to delimit the search range of the MLE cost function evaluation, from which a final estimation is obtained. The complexity of this technique is reduced by considering the cost function simplifications presented in [1].

Finally, a quadratic interpolation is used in both cases to obtain refined estimates [11].

We note that in case b) a previous distinction from the single-target scenario has to be assumed, where simple methods, such as described in [5], can be applied.

The remaining thesis is organized as follows. In Chapter 2, we formulate the DOA estimation problem for two targets in the single-snapshot case. The BF method, the MLE for two targets and the corresponding proposed improvements are presented in Chapter 3, where also the mentioned iterative algorithms are briefly described. A possible overall DOA estimation procedure is proposed in Chapter 5. The performance comparison, in terms of RMSE and computational cost, is shown in Chapter 5. The conclusions are finally exposed in Chapter 6.

2 Problem Formulation

In this section, the signal model is provided for the single- and the two-target scenario. Since the interest of the thesis is focused on situations in which a single snapshot is only available, both data models are presented for a single snapshot.

2.1 Parametric Data Model

Consider an array, composed of M sensors with uniform linear distribution (M-ULA), and assume that a radar pulse impinges on it from a single-target reflection, where θ is the physical DOA of the target, as shown in Figure 2.1.

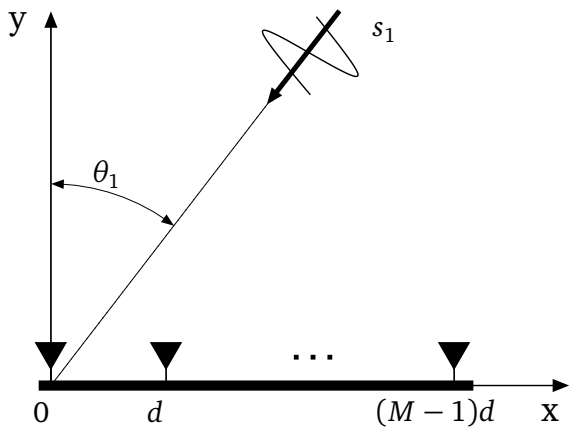

Figure 2.1: Uniform linear array composed of M elements in the single-target scenario.

In radar applications, and also in automotive radar, the array aperture is typically much smaller than the inverse relative bandwidth of the radar signal, therefore narrowband condition can be assumed to be valid [*]. The resulting array output vector $\mathbf{x}$ generated from a single-target reflection is given by

$$\mathbf{x} = \mathbf{a}(\phi_1)s_1, \tag{2.1}$$

where s_1 and ϕ_1 are the complex target response parameter and DOA parameter, respectively, and

$$\mathbf{a}(\phi) = \frac{1}{\sqrt{M}}[1, e^{j\phi}, \ldots, e^{j\phi(M-1)}]^T$$

is the normalized ULA steering vector [3]. $\phi = kd\sin(\theta)$ is the electrical angle, $k = \frac{2\pi}{\lambda}$ is the wavenumber, λ is the wavelength and d is the array element spacing.

[*] *We assume narrowband conditions when the physical size of the array, measured in wavelengths, is much less than the inverse relative bandwidth:* $\frac{d}{\lambda} \ll \frac{f_o}{B_o}$. *In typical radar applications* $\frac{d}{\lambda} \approx 1$ *and* $\frac{f_o}{B_o} \approx 10^3$ *[6]*

In the presence of additive noise, the expression in (2.1) takes the form

$$\mathbf{x} = \mathbf{a}(\phi_1)s_1 + \mathbf{n}, \tag{2.2}$$

where noise vector $\mathbf{n}$ is assumed to be spatially white, circular complex Gaussian distributed, with zero mean and common variance σ^2.

In addition to the single-target scenario, the two-target case is also relevant for DOA estimation in automotive radar applications. This situation usually occurs when a ghost target is introduced in the system due to specular multipath with the guardrail.
Then, the expression for the array output vector is obtained by inserting a second target into (2.2)

$$\mathbf{x} = \mathbf{a}(\phi_1)s_1 + \mathbf{a}(\phi_2)s_2 + \mathbf{n}, \tag{2.3}$$

which can also be formulated in compact form as

$$\mathbf{x} = \mathbf{A}(\phi_1, \phi_2)\mathbf{s} + \mathbf{n}, \tag{2.4}$$

where $\mathbf{A}(\phi_1, \phi_2) = [\mathbf{a}(\phi_1), \mathbf{a}(\phi_2)]$ is the steering matrix and $\mathbf{s} = [s_1, s_2]$ denotes the vector of target response parameters.

3 DOA Estimation for Two Targets

The conventional beamformer (BF) is the simplest technique for DOA estimation, data preprocessing is not required and an efficient implementation is also possible using the FFT.
However, the estimates obtained in the two-target case are often biased, and furthermore, the BF is unable to resolve closely spaced targets, due to its resolution limit.

In this Chapter, after briefly introducing the BF, two improvements are proposed in order to exploit the advantages of the BF in resolved scenarios. The first makes it possible to reduce the bias by using a look-up table, and the second minimizes the number of points to evaluate, through the use of a parabolic approximation. Afterwards, the MLE for two targets is presented and we briefly describe a simplified implementation, from which can be used as a high-resolution method for non-resolved situations.
For performance comparison with other algorithms, we finally present three iterative techniques: the RELAX algorithm, the method of alternating projections (AP) and the Alternating Notch Periodogram algorithm (ANP). All of them are computationally practicable implementations of the MLE and do not require an eigendecomposition.

3.1 The Conventional Beamformer

The BF method consists of maximizing the array output power when the aperture is steered to the true direction. Given the output vector $\mathbf{x}$ with single target from ϕ according to (2.2), the array response is given by

$$\mathbf{y} = \mathbf{w}^H \mathbf{x}, \tag{3.1}$$

where $\mathbf{w}$ is the array weighting vector. Constraining the norm of $\mathbf{w}$ to be unity and maximizing the power of (3.1), we obtain the well-known solution

$$P(\phi) = |\mathbf{a}(\phi)^H \mathbf{x}|^2, \tag{3.2}$$

which is the spatial equivalent to the periodogram in spectral analysis [12].

The BF technique performs efficiently in the single-target case. But in contrast, when we deal with the two-target case, the method yields biased estimates and is not able to resolve closely spaced targets, regardless of the SNR.

The BF resolution is limited by the beamwidth $BW = \frac{2\pi}{M}$, and consequently, by the array aperture size. Therefore, high-resolution techniques are required for situations in which the targets' separation is lower than the BF resolution limit, i.e., $|\phi_2 - \phi_1| < BW$. An example is illustrated in Figure 3.1.

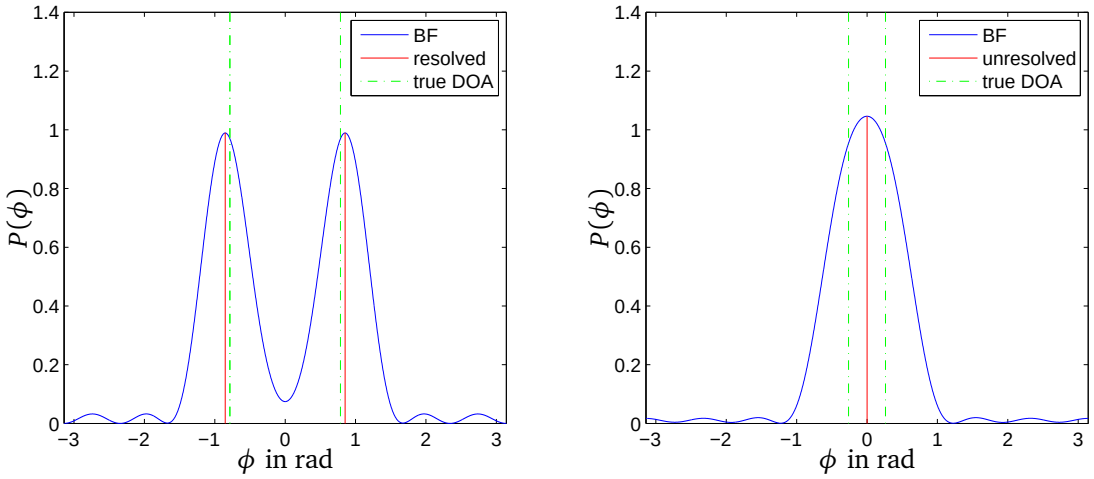

Figure 3.1: BF spectrum example for resolved (left) and non-resolved (right) two-target scenario, targets are separated by $|\phi_2 - \phi_1| = 2BW$ and $|\phi_2 - \phi_1| = 0.5BW$, respectively.

3.1.1 BF for Two Targets

In this section, the behavior of the BF is analyzed for the two-target scenario. But before going into detail, some definitions are made in order to simplify further notation.

From (3.2), we first define the Spatial Fourier transform $S(\phi)$ as

$$S(\phi) = \mathbf{a}(\phi)^H \mathbf{x}, \tag{3.3}$$

then, we proceed to evaluate (3.3) for the two-target case, but as an exception, we consider the noise-free case:

$$S(\phi) = \mathbf{a}(\phi)^H \mathbf{a}(\phi_1) s_1 + \mathbf{a}(\phi)^H \mathbf{a}(\phi_2) s_2. \tag{3.4}$$

This exception is made for the purpose of evaluating only the contribution of targets, irrespective of the noise. Thus, we can more easily identify how to improve the method.

We continue by defining the steering weighting function $W(\phi - \phi_i)$, or shifted beam pattern [10], as

$$W(\phi - \phi_i) = \mathbf{a}(\phi)^H \mathbf{a}(\phi_i) = \frac{1}{M} \sum_{m=0}^{M-1} e^{j(\phi - \phi_i)m}, \tag{3.5}$$

and using the finite geometric series and the sine definition as a sum of complex exponentials, (3.5) can be re-written as

$$W(\phi - \phi_i) = \frac{1}{M} \frac{\sin((\phi - \phi_i)\frac{M}{2})}{\sin((\phi - \phi_i)\frac{1}{2})} e^{-j(\phi - \phi_i)\frac{M-1}{2}}. \tag{3.6}$$

Using the notation above, we can formulate the BF spectrum for two targets, ignoring the presence of noise, as

$$\begin{aligned} P(\phi) &= |S(\phi)|^2 \\ &= |s_1|^2|W(\phi-\phi_1)|^2 + |s_2|^2|W(\phi-\phi_2)|^2 + 2Re\{s_1 s_2^* W(\phi-\phi_1)W(\phi-\phi_2)^*\} \end{aligned} \tag{3.7}$$

where the first two terms are the target contributions and the third term is a cross-term contribution.

The BF has been designed for DOA estimation of a single target. Thus, it is not optimal for two targets and we have to deal with leakage and cross-terms.

We can define the cross product of the steering weighting function as

$$Q_{12}(\phi) = W(\phi-\phi_1)W(\phi-\phi_2)^* = Q_{12,mag}(\phi)e^{j\angle Q_{12}(\phi)} \tag{3.8}$$

where $Q_{12,mag}$ is a real-valued function.

Noting that the phase of $Q_{12}(\phi)$ can be easily calculated by computing

$$\angle Q_{12}(\phi) = \angle W(\phi-\phi_1) - \angle W(\phi-\phi_2) = (\phi_1-\phi_2)\frac{M-1}{2},$$

the cross-term contribution from (3.7) can be characterized by using the definition stated in (3.8), as

$$P(\phi)_{cross-term} = 2|s_1||s_2|Q_{12,mag}(\phi)\cos((\angle s_1 - \angle s_2) + (\phi_1-\phi_2)\frac{M-1}{2}). \tag{3.9}$$

This result is crucial to detect which factors affect the bias of the BF estimates. Actually, it is the basis to understand the improvement described in the following section.

3.1.2 BF using Look-Up Table

As a result of (3.9), when we estimate using the BF in the two-target case, we have that the bias obtained not only depends on the angular separation between DOA parameters, but also on the phase difference between the target response parameters.

Considering $\phi_2 > \phi_1$, and using notation $\delta = \phi_2 - \phi_1$, $\varphi = \angle s_2 - \angle s_1$ and $\alpha = \frac{|s_2|}{|s_1|}$ for convenience, we can formulate an array output vector depending on these parameters as

$$\mathbf{x}(\varphi,\delta,\alpha) = \mathbf{a}(-\frac{\delta}{2}) + \alpha e^{j\varphi}\mathbf{a}(\frac{\delta}{2}) \tag{3.10}$$

where the noise-free case is also considered.

Thereby, the bias of the BF estimates corresponding to the parameters δ, φ and α can be expressed as

$$\begin{aligned} L_1(\varphi,\delta,\alpha) &= \phi_1 - \hat{\phi}_{1,BF}(\varphi,\delta,\alpha) \\ L_2(\varphi,\delta,\alpha) &= \phi_2 - \hat{\phi}_{2,BF}(\varphi,\delta,\alpha) \end{aligned} \tag{3.11}$$

where $\hat{\phi}_{1,BF}(\varphi,\delta,\alpha)$ and $\hat{\phi}_{2,BF}(\varphi,\delta,\alpha)$ are the BF estimates for the array output vector $\mathbf{x}(\delta,\varphi,\alpha)$, and where it is also considered $\hat{\phi}_{2,BF} > \hat{\phi}_{1,BF}\ \forall\ \varphi,\delta,\alpha$.

Assuming α to be constant, we proceed to evaluate the functions defined in (3.11) by varying φ and δ. Since we are focused on resolved scenario, we have to evaluate δ for higher values than the BF resolution limit, but also for lower values than $2\pi - BW = (M-1)BW$, due to the 2π-periodicity of the BF spectrum. Therefore, we consider $\delta \in [BW,(M-1)BW]$.
The phase difference has to be evaluated for $\varphi \in [-\pi,\pi)$.

Figure 3.2 shows the tables obtained by evaluating L_1, L_2 (left, right) for scalars $\alpha = 1$ (top), 0.85 (center) and 0.7 (bottom). We have considered a ULA with $M = 8$ elements and the grid parameters described above, with step sizes $\Delta\varphi = \frac{2\pi}{120}$ and $\Delta\delta = \frac{2\pi}{160}$.
As we can observe, for $\alpha = 1$ the bias of the estimates $\hat{\phi}_{1,BF}$ and $\hat{\phi}_{2,BF}$ are reciprocals but with the sign changed, i.e., $L_2(\varphi,\delta,1) = -L_1(\varphi,\delta,1)$. For the other values of α, the tables obtained have the same distribution as for $\alpha = 1$, but the intensity of the biases is different. Actually, we have that

$$\begin{aligned} L_1(\varphi,\delta,\alpha) &= \alpha L(\varphi,\delta) \\ L_2(\varphi,\delta,\alpha) &= -\tfrac{1}{\alpha} L(\varphi,\delta) \end{aligned}$$

where $L(\varphi,\delta) = L_1(\varphi,\delta,1)$.

This result can be deduced from (3.9), since the cross term is scaled by the factor $|s_1||s_2|$. Therefore, it is only necessary the evaluation of $L(\varphi,\delta)$ to get the bias of $L_1(\varphi,\delta,\alpha)$ and $L_2(\varphi,\delta,\alpha)$.

Another important fact to note are the values of all the tables at both the upper and lower left corners. The scalars obtained at these areas show that the BF is not able to estimate properly for the corresponding values of φ and δ. The BF spectrum obtained evaluating these points is similar than in non-resolved case, i.e., only a single main beam with beamwidth $> BW$ is present in the spectrum. Therefore, these correction factors will be set to 0, in order not to introduce more errors.

The key idea for reducing the bias is to compute $L(\varphi,\delta)$ off-line for every point of interest, φ and δ, and store them into a look-up table (LUT). When estimating in the resolved case, we can correct the bias of the BF estimates by using the LUT.

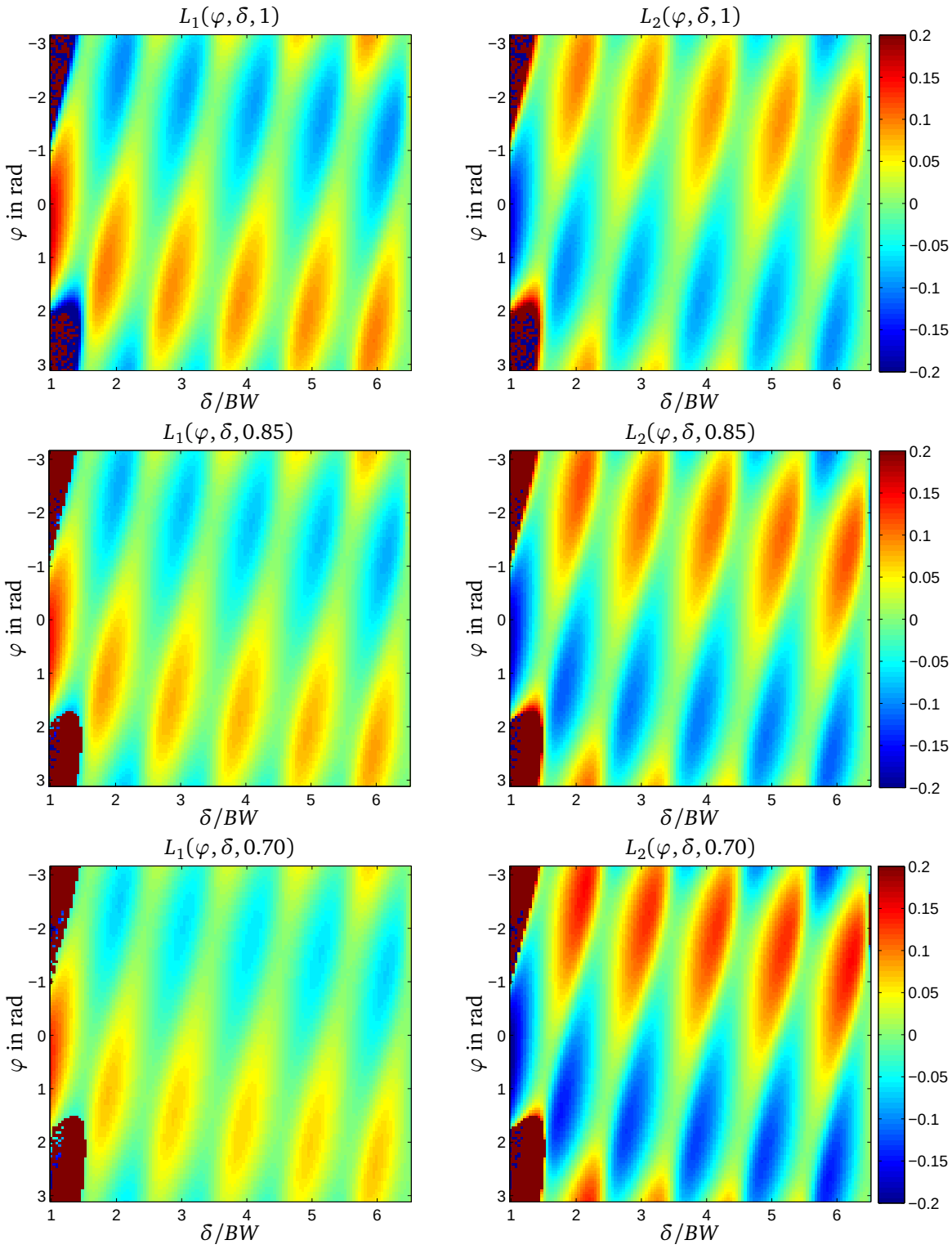

Figure 3.2: Evaluation of the BF bias functions $L_1(\varphi, \delta, \alpha)$, $L_2(\varphi, \delta, \alpha)$ (left, right), considering a ULA with $M = 8$ elements. The target response parameters are constrained to $\alpha = 1$ (top), 0.85 (center) and 0.70 (bottom).

Given the array output vector $\mathbf{x}$ composed of two targets according to (2.4), we apply the bias correction as follows.

Step 1) Estimate the DOA parameters by using the BF, obtaining

$$\hat{\phi}_{1,BF},\ \hat{\phi}_{2,BF}$$

Step 2) Estimate the target response parameters as [4]

$$\hat{s}_i = \mathbf{a}(\hat{\phi}_{i,BF})^H \mathbf{x}\ ,\ \ i = 1,2$$

Step 3) Compute the estimation of the LUT parameters by

$$\begin{aligned} \hat{\varphi} &= \angle\hat{s}_2 - \angle\hat{s}_1 \\ \hat{\delta} &= \hat{\phi}_{2,BF} - \hat{\phi}_{1,BF} \\ \hat{\alpha} &= \frac{|\hat{s}_2|}{|\hat{s}_1|} \end{aligned}$$

Step 4) Get the indexes of the LUT corresponding to the φ and δ which are closest to the estimates, i.e,

$$\begin{aligned} n_{\text{opt}} &= \arg\min_n \{\, |\varphi_n - \hat{\varphi}| \,\} \\ q_{\text{opt}} &= \arg\min_q \{\, |\delta_n - \hat{\delta}| \,\} \end{aligned}$$

Step 5) Apply the correction factor to the BF DOA estimates

$$\begin{aligned} \hat{\phi}_{1,\text{BF+LUT}} &= \hat{\phi}_{1,\text{BF}} + \hat{\alpha} L(\hat{\varphi}_{n_{\text{opt}}}, \hat{\delta}_{q_{\text{opt}}}) \\ \hat{\phi}_{2,\text{BF+LUT}} &= \hat{\phi}_{2,\text{BF}} - \tfrac{1}{\hat{\alpha}} L(\hat{\varphi}_{n_{\text{opt}}}, \hat{\delta}_{q_{\text{opt}}}) \end{aligned}$$

where $\hat{\phi}_{1,\text{BF+LUT}}$ and $\hat{\phi}_{2,\text{BF+LUT}}$ are the refined DOA estimates.

3.1.3 Parabolic Approximation

The DOA estimates are obtained by locating the peaks of the BF spectrum $P(\phi)$, formulated in (3.2). The spectrum is generally evaluated on a discrete grid with step size $\Delta\phi$, which set the resolution for locating the peaks.

The idea of the improvement is to approximate the shape of the main beams of the BF spectrum with a parabolic function. Thus, we can obtain an estimation of the peak location via a quadratic interpolation, reducing considerably the number of points to evaluate [11].

The equation which defines the parabola with vertex at $(\phi_i, P(\phi_i))$ and focus at $(\phi_i, P(\phi_i) - P_0)$ takes the form

$$(\phi - \phi_i)^2 = 4P_0(P(\phi) - P(\phi_i)). \tag{3.12}$$

We can find ϕ_i by solving a system of equations, formed by the evaluation of (3.12) at three points located near to the peak. The result, solving for the DOA parameter ϕ_i, is given by

$$\hat{\phi}_i = \phi_{i,m} - \frac{\Delta\phi}{2} \frac{P(\phi_{i,m+1}) - P(\phi_{i,m-1})}{P(\phi_{i,m+1}) - 2P(\phi_{i,m}) + P(\phi_{i,m-1})}, \tag{3.13}$$

where $\phi_{i,m}$ is the initial estimation of the peak position and $\hat{\phi}_i$ is the refined peak location.

Given an M-ULA and referring to the BF spectrum, if we consider $\Delta\phi = \frac{BW}{2}$ as the largest possible step size, we can guarantee that at least we will obtain three representative points of a main beam, as it is illustrated in Figure 3.3.

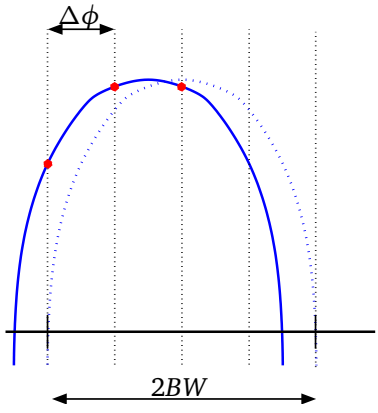

Figure 3.3: Possible samplings of a main beam from the BF spectrum, for M-ULA, step size $\Delta\phi = \frac{BW}{2}$ and $BW = \frac{2\pi}{M}$.

For an angular sector $\phi \in [\phi_{min}, \phi_{max}]$, the minimum number of points to evaluate is

$$N_{eval} = \frac{(\phi_{max} - \phi_{min})}{\Delta\phi} + 1 = M\frac{(\phi_{max} - \phi_{min})}{\pi} + 1. \tag{3.14}$$

Thus, only $2M$ points are required to evaluate the complete field-of-view.

While evaluating the BF spectrum in the two-target case, the parabolic shape better approximates the main beams when the power is expressed in dB. Therefore, we use the logarithm of the BF spectrum $10\log_{10}(P(\phi))$ in the following.

Figure 3.5 illustrates the performance of the parabolic approximation. We consider a ULA with $M = 8$ elements in the two-target case, and we evaluate the BF spectrum for $2M$ samples (blue lines). Markers '*' and 'o' correspond to the points used to apply the method for the first and the second target, respectively, as it is described in (3.13). The red lines correspond to the obtained peaks.
The BF spectrum is also evaluated for 1000 samples (green lines), in order to contrast the results.

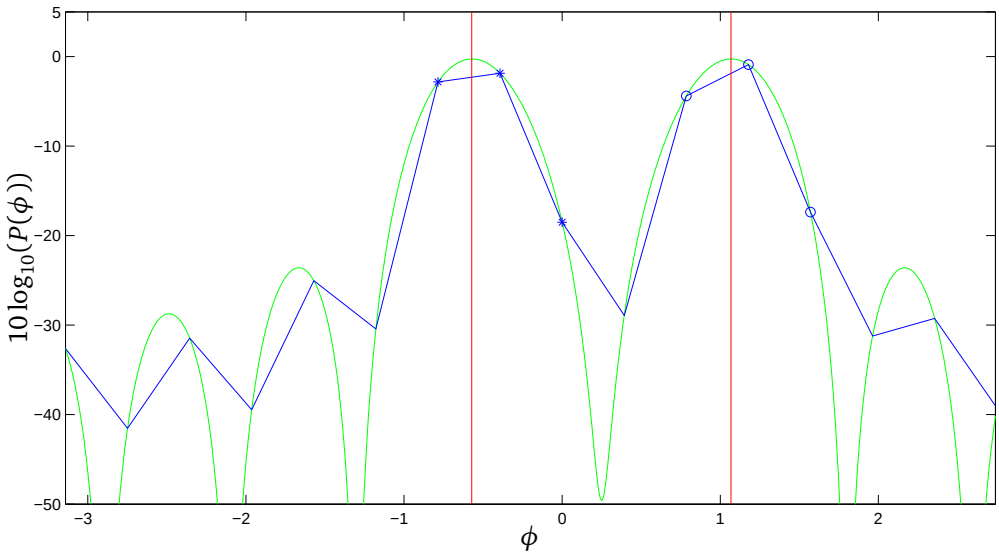

Figure 3.4: BF spectrum of 8-ULA for $2M$ samples (blue lines) and 1000 samples (green lines). The refined peaks (red lines) are obtained by the parabolic approximation of points '*' and 'o', respectively.

As we can observe, the parabolic approximation gives an accurate location of the corresponding peaks, by using only $2M$ samples of the BF spectrum.

3.2 MLE for DOA parameters

For DOA parameters $\Phi = [\phi_1, \cdots, \phi_K]$, where K denotes the number of targets to estimate, the maximum likelihood estimator is given by the global minimum of the following trace argument [10]

$$\arg\min_{\Phi} \{ Tr[\mathbf{P}_A^{\perp}(\Phi)\hat{\mathbf{R}}] \} \tag{3.15}$$

where $\hat{\mathbf{R}} = \mathbf{x}\mathbf{x}^H$ is the sample covariance matrix, and $\mathbf{P}_A^{\perp} = \mathbf{I} - \mathbf{P}_A$ denotes the orthogonal projection of the steering matrix $\mathbf{A}$, i.e.,

$$\mathbf{P}_A = \mathbf{A}(\mathbf{A}^H\mathbf{A})^{-1}\mathbf{A}^H \tag{3.16}$$

using notation $\mathbf{A} = \mathbf{A}(\Phi)$ and $\mathbf{P}_A = \mathbf{P}_A(\Phi)$ for convenience.

We can interpret (3.15) as a minimization problem of power measurement, where data vector $\mathbf{x}$ has been projected onto the orthogonal space defined by the columns of the steering matrix $\mathbf{A}$.
As a consequence, the minimum will be measured when the projection removes all the signal components, and that occurs when the projection is orthogonal to

$$\mathbf{a}(\phi_1), \cdots, \mathbf{a}(\phi_K) \tag{3.17}$$

where $\phi_1, \cdots, \phi_K$ are the true DOA parameters.

We can also turn (3.15) into a maximization problem, by using $\mathbf{P}_A$ instead of the orthogonal $\mathbf{P}_A^{\perp}$:

$$\arg\max_{\Phi} \{ Tr[\mathbf{P}_A(\Phi)\hat{\mathbf{R}}] \}. \tag{3.18}$$

Now, the power measurement will be maximum when the space, onto which data are projected, is spanned by (3.17).

In order to continue simplifying (3.18), we can exploit the cyclic permutation property of the trace operation, as applied below

$$Tr[\mathbf{P}_A(\Phi)\hat{\mathbf{R}}] = Tr[\mathbf{P}_A(\Phi)\mathbf{x}\mathbf{x}^H] = Tr[\mathbf{x}^H\mathbf{P}_A(\Phi)\mathbf{x}].$$

Since trace of a scalar is a scalar, the cost function to maximize of (3.18) can be re-formulated as

$$c(\Phi) = \mathbf{x}^H\mathbf{P}_A(\Phi)\mathbf{x}. \tag{3.19}$$

3.2.1 MLE for Single Target

For the particular case of single target, we have that the steering matrix contains only a single steering vector $\mathbf{A}(\Phi) = \mathbf{a}(\phi)$, thus, the projection matrix takes the form:

$$\mathbf{P}_A(\phi) = \mathbf{a}(\phi)[\mathbf{a}(\phi)^H\mathbf{a}(\phi)]^{-1}\mathbf{a}(\phi)^H = \mathbf{a}(\phi)\mathbf{a}(\phi)^H.$$

If we evaluate (3.19) for this case, we have

$$c(\phi) = \mathbf{x}^H\mathbf{a}(\phi)\mathbf{a}(\phi)^H\mathbf{x} = |\mathbf{a}(\phi)^H\mathbf{x}|^2$$

Thus the BF is actually the maximum likelihood estimator for DOA parameter ϕ [3], for a single target.

3.2.2 MLE for Two Targets

In the two-target case, the evaluation of the cost function is not as simple as for a single target. In order to compute the projection matrix $\mathbf{P}_A$, the inversion of $\mathbf{A}^H\mathbf{A}$ is first required, where $\mathbf{A}$ is now composed of two steering vectors.

For $\mathbf{B} = \mathbf{A}^H\mathbf{A} \in \mathbb{C}^{2\times 2}$, we have

$$\mathbf{B} = \begin{pmatrix} 1 & \beta \\ \beta & 1 \end{pmatrix},$$

where $\beta = \mathbf{a}_1^H\mathbf{a}_2$ and using that $\mathbf{a}_1^H\mathbf{a}_1 = \mathbf{a}_2^H\mathbf{a}_2 = 1$. Since the inversion formula can be applied easily for 2-by-2 matrices, the computation of $\mathbf{B}^{-1}$ is given by

$$\mathbf{B}^{-1} = \frac{1}{1-|\beta|^2}\begin{pmatrix} 1 & -\beta \\ -\beta^* & 1 \end{pmatrix}, \tag{3.20}$$

and inserting (3.20) into (3.16), we obtain

$$\mathbf{P}_A = \frac{1}{1-|\beta|^2}(\mathbf{a}_1\mathbf{a}_1^H - \beta\mathbf{a}_1\mathbf{a}_2^H - \beta^*\mathbf{a}_2\mathbf{a}_1^H + \mathbf{a}_2\mathbf{a}_2^H).$$

Finally, we can use the simplified expression above to re-write the cost function described in (3.19). Thereby, the cost function in the two-target case takes the form

$$c(\phi_1,\phi_2) = \mathbf{x}^H\mathbf{P}_A(\phi_1,\phi_2)\mathbf{x} = \frac{1}{1-|\beta|^2}(|\alpha_1|^2 - 2Re\{\beta\alpha_1\alpha_2^*\} + |\alpha_2|^2) \tag{3.21}$$

where $\alpha_1 = \mathbf{a}_1^H\mathbf{x}$ and $\alpha_2 = \mathbf{a}_2^H\mathbf{x}$.

In contrast to the BF estimation in the two-target scenario, the MLE requires a two-dimensional search over a given grid, demanding more expensive computations for the cost function evaluation. However, the situations in which high-resolution techniques are required motivate the use of MLE-based methods, owing its optimum capability to resolve them.

Nevertheless, as we will see in the following section, the evaluation of the MLE cost function also admits simplifications which reduce considerably the computational cost.

3.2.3 Global Search

The Global Search is a direct implementation of the MLE cost function evaluation. In the two-target case and given a two-dimensional grid, the algorithm consists of computing $c(\phi_i,\phi_j)$ for each point of the grid, obtaining the DOA estimates by locating the global maximum.

The Figure below illustrates the MLE cost function evaluation, considering a ULA with $M = 8$ elements and two targets separated by $|\phi_2 - \phi_1| = 0.5BW$. The global maximum is indicated with a dotted cross and the star corresponds to the true DOA parameters.

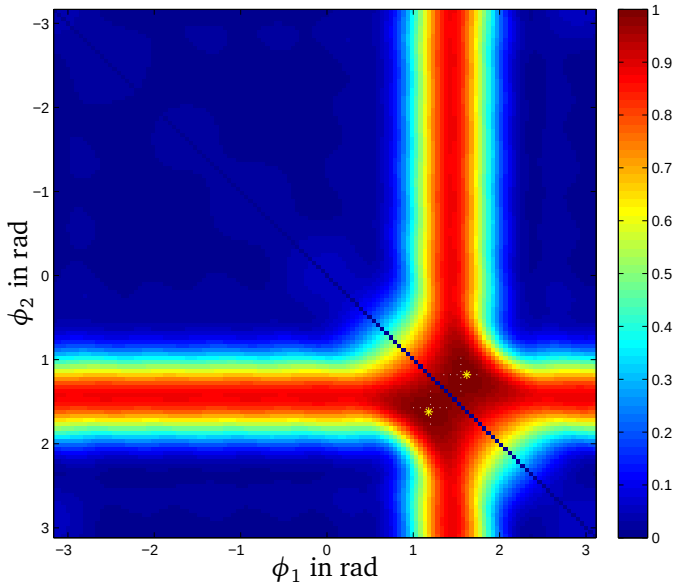

Figure 3.5: Normalized MLE cost function evaluation for a ULA with $M = 8$ elements and two targets, with $|\phi_2 - \phi_1| = 0.5BW$ and $\Delta\phi = \frac{2\pi}{96}$. It is illustrated the true DOA parameters (star) and the global maximum (dotted cross).

The first trivial improvement is to evaluate only the triangular area defined by $\phi_1 < \phi_2$, since the computation of $c(\phi_1, \phi_2)$ and $c(\phi_2, \phi_1)$ produce the same result. Therefore, the number of points to evaluate is reduced to

$$S_2 = \frac{N_{eval}(N_{eval} - 1)}{2}$$

where N_{eval} is the number of grid points at each dimension.

Continuing with reducing the area to evaluate, we can delimit the search range by using the information of the BF spectrum. For two targets with similar powers in non-resolved case, the evaluation of the BF spectrum is characterised by having a single main beam, due to the resolution limit. The peak may occur at an intermediate point between the targets location, since it is produced because of the superposition of both contributions.
We can exploit this property by delimiting the search range to the area surrounding the peak. When we extend the search perimeter to BW, the number of evaluations is reduced significantly.

As in the case of the BF estimation, we can also use the parabolic approximation to obtain a refined peak of the global maximum. Despite being a two-dimensional paraboloid function, we can solve for each dimension separately by applying the method described in Section 3.1.3.

In [1], we can find a further analysis of the improvements described above: a more formal definition of delimiting the search range is given by using a rotational shift of the field-of-view, and two simplified cost functions are also proposed, which make it possible to reduce the computational burden.

To be precise, we consider the simplification from [1] which not employs an eigendecomposition: using a unitary transformation, the covariance matrix and the projection matrix are reduced to real-valued matrices $\hat{\mathbf{C}}$ and $\mathbf{V}(\phi_1, \phi_2)$, respectively, where the centro-hermitian property of the forward-backward (FB) averaged covariance matrix is used. This method exploits the symmetry of both matrices to simplify the evaluation of the MLE cost function to

$$c(\phi_1, \phi_2) = Tr\{\mathbf{V}(\phi_1, \phi_2)\hat{\mathbf{C}}\} = \mathbf{v}(\phi_1, \phi_2)^T \hat{\mathbf{c}}$$

where $\mathbf{v}(\phi_1, \phi_2)$ and $\hat{\mathbf{c}}$ are the vectorization of the non-redundant elements from matrices $\hat{\mathbf{C}}$ and $\mathbf{V}(\phi_1, \phi_2)$. Noting that $\hat{\mathbf{c}}$ has to be computed only once, the author propose to pre-calculate off-line and store the projection operators $\mathbf{v}(\phi_1, \phi_2)$. Thereby, this simplification reduces the computation of the MLE cost function to only $S_1 = \frac{M(M+1)}{2}$ real-valued multiply-add operations. The required storage space depends on the total number of points to evaluate, which in turn is defined by the step size.

3.3 Iterative Algorithms

In this section, three iterative implementations of the MLE are presented: the RELAX algorithm, the method of alternating projections and the Alternating Notch Periodogram algorithm. A brief description for both techniques is given below.

3.3.1 RELAX algorithm

The main goal of the RELAX algorithm is to transform a multiple-target estimation problem into an iterative sequence of single-target estimation problems, which can be efficiently solved using the BF.

Given the array output vector $\mathbf{x}$ composed of K sources, single-target output vectors $\mathbf{x}_1, \cdots, \mathbf{x}_K$ are generated by proceeding as described below:

$$\mathbf{x}_k = \mathbf{x} - \sum_{i=1, i\neq k}^{K} \hat{s}_i \mathbf{a}(\hat{\phi}_i) \quad , \quad k = 1, \cdots, K \tag{3.22}$$

where $\hat{s}_i$ and $\hat{\phi}_i$ are, respectively, the estimates of the target response parameter and the DOA parameter of source i. The target response parameter is estimated by using

$$\hat{s}_k = \mathbf{a}(\hat{\phi}_k)^H \mathbf{x}_k \quad , \quad k = 1, \cdots, K. \tag{3.23}$$

As it is described in [4], both (3.22) and (3.23) correspond to the minimization of the following nonlinear least-squares (NLS) criterion:

$$c_{NLS} = \| \mathbf{x} - \sum_{i=1}^{K} s_i \mathbf{a}(\phi_i) \|^2 . \tag{3.24}$$

In the two-target case, the algorithm proceeds as follows. Initially, it is assumed to be a single target and we consider $\mathbf{x}_1 = \mathbf{x}$, from which $\hat{\phi}_1$ is obtained by locating the global maximum of the BF spectrum. The target response parameter $\hat{s}_1$ is estimated as described in (3.23).
Once the first target is estimated, we are able to generate $\mathbf{x}_2$ by using (3.22), in order to estimate the parameters of the second target as the same way as for the first target.
In the following iterations, "cleaner" output vectors $\mathbf{x}_1$ and $\mathbf{x}_2$ are produced, which, in turn, makes it possible to reduce the bias while estimating with the BF, because of its optimal performance in the single-target case.

Therefore, the algorithm requires a higher number of iterations to yield accurate estimates when the targets are closely spaced, since the "cleaning" process is less effective for these situations, due to the behaviour of the BF in non-resolved case. However, the computational cost at each iteration is much less than the computations required to calculate the MLE cost function.

The RELAX algorithm can also take advantage of the quadratic interpolation, proposed for obtaining the global maximum of the BF spectrum.

3.3.2 Alternating Projection method and Alternating Notch Periodogram algorithm

Both the AP and ANP techniques are based on a similar simplification concept as the RELAX algorithm: turn the multi-dimensional maximization of the MLE cost function into multiple one-dimensional maximization problems.
However, whereas the first algorithm exploits each iteration to refine the initial estimation, the two methods presented in this section iterate to find the global maximum of the MLE cost function, avoiding the evaluation of all the grid points.

This technique, also known as "deterministic hill climbing", provides a much simpler estimation of the global maximum than the Global Search, nevertheless the global convergence is not guaranteed [14].

The multi-dimensional cost function evaluation is simplified by varying only one DOA parameter at a time, while fixing the other DOA parameters to their previously estimated values. This process requires an important initialization step, which is simply solved for both algorithms by

$$\begin{aligned}
\hat{\phi}_1^{(0)} &= \arg\min_{\phi_1} \{\, Tr[\mathbf{P}_A([\phi_1])\mathbf{R}] \,\} \\
\hat{\phi}_2^{(0)} &= \arg\min_{\phi_2} \{\, Tr[\mathbf{P}_A([\hat{\phi}_1^{(0)}, \phi_2])\mathbf{R}] \,\} \\
&\cdots \\
\hat{\phi}_K^{(0)} &= \arg\min_{\phi_K} \{\, Tr[\mathbf{P}_A([\hat{\phi}_1^{(0)}, \hat{\phi}_2^{(0)}, \cdots, \hat{\phi}_{K-1}^{(0)}, \phi_K])\mathbf{R}] \,\}
\end{aligned}$$

where K denotes the number of targets, and $\mathbf{P}_A(\Phi)$ is the projection matrix defined in (3.16).

As it is introduced above, K 1-D evaluations of the MLE cost function are produced at each iteration. Considering iteration n, the DOA estimates are given by

$$\hat{\phi}_i^{(n)} = \arg\min_{\phi_i} \{\, Tr[\mathbf{P}_A([\phi_i, \Phi_i^{(n)}])\mathbf{R}] \,\} \quad , \quad i = 1, \cdots, K$$

where $\Phi_i^{(n)} = [\hat{\phi}_1^{(n)}, \cdots, \hat{\phi}_{i-1}^{(n)}, \hat{\phi}_{i+1}^{(n)}, \cdots, \hat{\phi}_K^{(n)}]$ is the vector containing the pre-estimated DOA parameters.

The main difference between algorithms AP and ANP is the way to compute $\mathbf{P}_A([\phi_i, \Phi_i])$: the first method uses a projection matrix decomposition to simplify its evaluation, and the second algorithm exploits concurrent Gram-Schmidt procedures, which allows its evaluation via FFT [2].
The ANP algorithm requires a greater computational burden, but nevertheless the results are expected to be better.

The improvements proposed for the Global Search can been applied likewise to the AP and ANP methods, since the concepts in which they are based are also present in both the two iterative algorithms.

4 DOA Estimation Block Diagram

In this Chapter, we present the procedure proposed to estimate the DOA parameters for single and two targets, considering the single-snapshot case.

Given the the array output vector **x** as defined in (2.4), the procedure consists of the following steps:

1. Analysis of the BF Spectrum resulting from **x**

   2a. Presence of a single main beam

   -a.3a Main beam suitable for the single-target case: the BF method is the maximum likelihood estimator
   $\Rightarrow \hat{\phi} = \hat{\phi}_{BF}$

   -a.3b Main beam suitable for the two-target case: use peak location to reduce the search range and apply the Global Search
   $\Rightarrow [\hat{\phi}_1, \hat{\phi}_2] = [\hat{\phi}_{1,GS}, \hat{\phi}_{2,GS}]$

   2b. Presence of two main beams

   -b.3 Use the BF DOA estimates to compute the LUT parameters and apply correction factors
   $\Rightarrow [\hat{\phi}_1, \hat{\phi}_2] = [\hat{\phi}_{1,BF+LUT}, \hat{\phi}_{2,BF+LUT}]$

As we can observe, the initial BF estimation is used in all cases to compute the final estimates, thus, the invested computation time is not in vain. In order to distinguish in 2a between the single- and the multiple-target case, a measurement of the beamwidth can be used. Nevertheless, an evaluation of the BF over a fine grid is required, thus making useless the parabolic approximation to reduce the number of evaluations.

In order to avoid this situation, we propose to use the criteria described in [5], which also allows to identify a single target, but without requiring a fine evaluation of the BF Spectrum. Its applicability is reduced to the single-snapshot case, which suits with the scenario considered in this thesis, and the computation involves simple operations over the array output vector **x**, which not overloads the final computational burden.

In the Figure 4.1, we present the recommended procedure for DOA estimation with one or two targets, in the single-snapshot case.

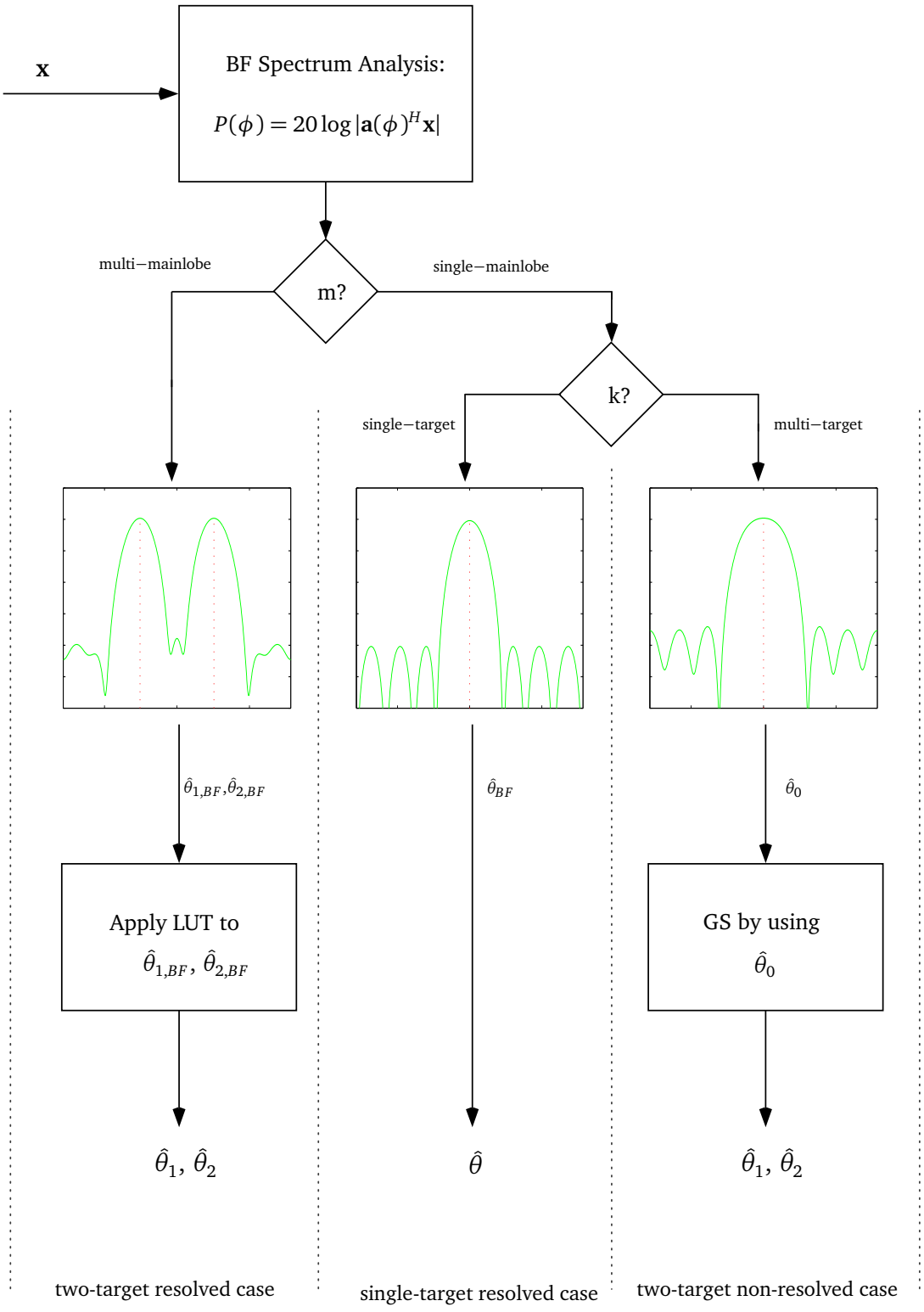

Figure 4.1: Block Diagram: DOA parameters estimation for one or two targets in the single-snapshot case.

5 Results

In this Chapter, we first describe the simulation setup for two-target DOA estimation, using a single snapshot. We then present the Cramér-Rao bound corresponding to the described scenario and comment the relevance of the step size.
Finally, the simulation results are shown and a further discussion of them is also given, considering both the resolved and the non-resolved case.

5.1 Simulation Model

We consider a ULA with $M = 8$ sensors, which are spaced by $d = \frac{\lambda}{2}$. Single snapshots are simulated for two target reflections with DOA parameters ϕ_1 and ϕ_2, as defined in model (2.4).

The targets are considered with random phases and, if not stated otherwise, similar magnitudes. To have a more realistic radar simulation setup, we use the following distributions:

$$|s_i| \sim 10^{0.1\,N(0,1)}, \quad \angle s_i \sim U[0, 2\pi), \quad i = 1, 2$$

where $N(0,1)$ is the Normal distribution with zero mean and standard deviation 1, and $U[a,b)$ is the uniform distribution between a and b.

The noise vector $\mathbf{n}$ is assumed to be spatially white, circular complex Gaussian distributed, with zero mean and common variance σ^2. The SNR is defined as $-20\log(\sigma)$ (dB).

In order to compute estimation errors, the physical DOA $\theta = \sin^{-1}(\frac{\phi}{kd})$ in degrees is used instead of the electrical angle. We consider the averaged root mean squared error (RMSE) as the performance index, which is given by

$$\overline{RMSE} = \sqrt{\frac{1}{MC}\sum_{m=1}^{MC}\frac{(\theta_1 - \hat{\theta}_{1,m})^2 + (\theta_2 - \hat{\theta}_{2,m})^2}{2}}$$

where $\hat{\theta}_{1,m}$ and $\hat{\theta}_{2,m}$ are the physical DOA estimates in Monte-Carlo iteration run m, and MC is the number of Monte-Carlo iterations, which is set to $MC = 1000$.

Regarding computational cost, the simulations have been conducted on a Windows PC with an AMD AthlonX2 processor at 1.80 GHz and 2 GB RAM. The average CPU times have been calculated by using functions tic and toc from MATLAB (version R2009a).

5.2 The Cramér-Rao bound

The Cramér-Rao bound (CRB) provides a lower bound on which can be used as an accuracy metric of the estimation algorithms. For DOA estimation of parameters ϕ_1 and ϕ_2 in the single-snapshot case, the CRB is given by [9]

$$\mathbf{CRB}_{\phi} = \frac{\sigma^2}{2}(Re\{\mathbf{S}^H\mathbf{D}^H\mathbf{P}_A^{\perp}\mathbf{D}\mathbf{S}\})^{-1}$$

where $\mathbf{S} = diag\{s_1, s_2\}$ is the diagonal matrix of the target response parameters, $\mathbf{D} = [\mathbf{d}(\phi_1), \mathbf{d}(\phi_2)]$ is the differential steering matrix with $\mathbf{d}(\phi) = \frac{\partial}{\partial\phi}\mathbf{a}(\phi)$, and $\mathbf{P}_A^{\perp}$ is the orthogonal projection of the steering matrix $\mathbf{A}$, which is defined in (3.15). As mentioned above, we use the physical angle to calculate estimation errors, therefore $\mathbf{CRB}_{\theta}$ should be used instead:

$$\mathbf{CRB}_{\theta} = \mathbf{G}^{-1}\mathbf{CRB}_{\phi}\mathbf{G}^{-1}$$

where $\mathbf{G} = diag\{kd\cos(\theta_1), kd\cos(\theta_2)\}$ is the transformation matrix.

5.3 Effect of the step size

The step size $\Delta\phi$ not only determines the estimation accuracy, but it also affects the computational cost. Therefore, we simulate each scenario for different values of $\Delta\phi$, in order to be able to contrast the results and establish a compromise between them.

5.4 Performance Comparison

The simulation results are divided into the resolved and the non-resolved scenario. The following parameters and algorithm settings are assumed for each case:

i) Resolved scenario:

- Angular separation $\phi_2 - \phi_1 \in [BW, (M-1)BW]$
- BF+LUT is computed by using a 128-by-128 lookup table
- Convergence condition $\epsilon = 10^{-3}$ (iterative algorithms)
- Number of steps limited to 3 (iterative algorithms)

ii) Non-resolved scenario:

- Angular separation $\phi_2 - \phi_1 \in [0.1BW, 2BW]$
- Convergence condition $\epsilon = 10^{-3}$ (iterative algorithms)
- Maximum number of steps limited to 10 (iterative algorithms)

where the convergence condition ϵ is considered as described in [4], [13] and [2] for the RELAX algorithm, the alternating projection method and the ANP algorithm, respectively.

5.4.1 Resolved scenario

A performance comparison, averaged RMSE versus angular separation, is given in the Figure below. The step size is set to $\Delta\phi = \frac{2\pi}{16}$ (top) and $\Delta\phi = \frac{2\pi}{32}$ (bottom), both with SNR $= 32$ dB.

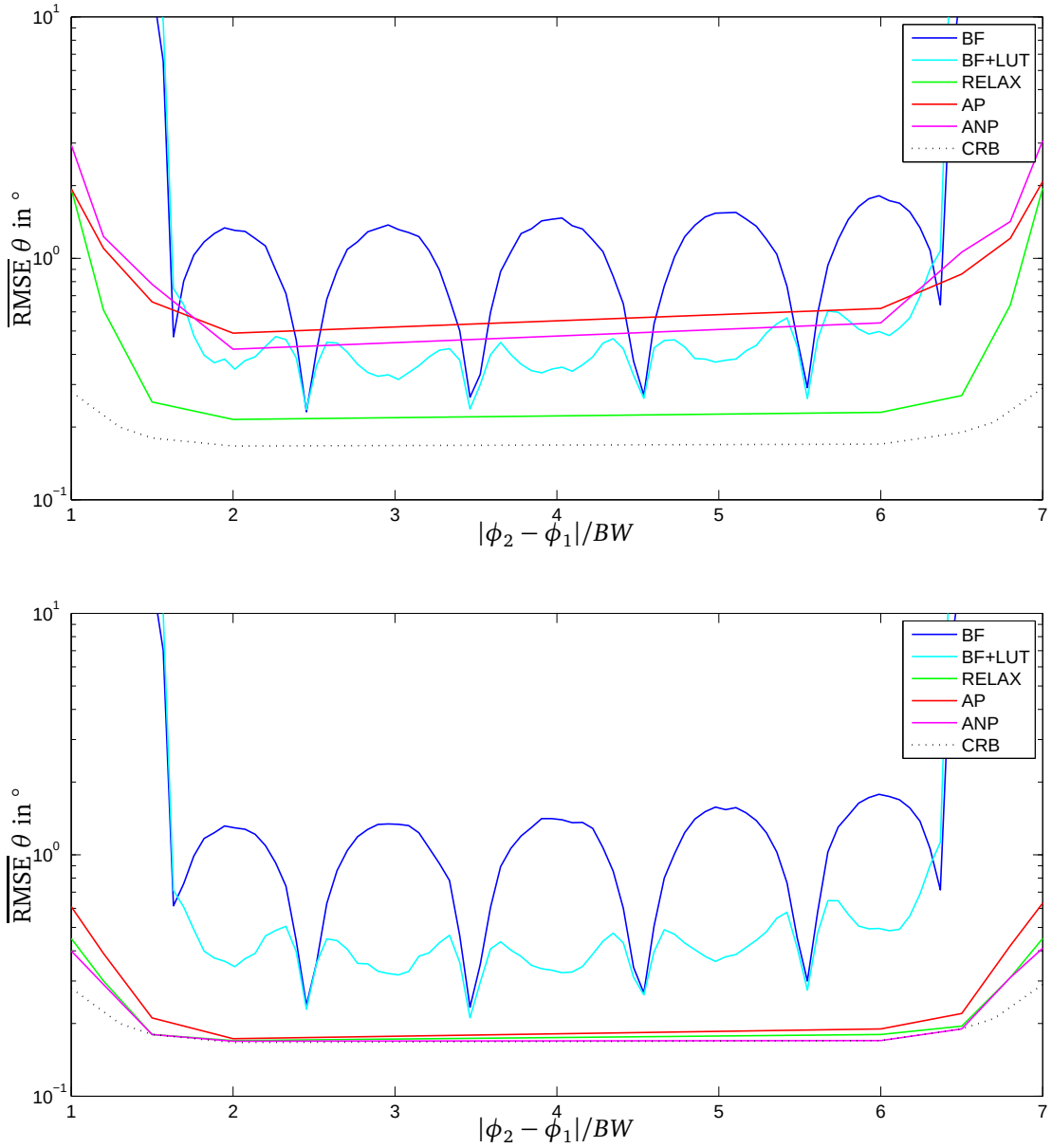

Figure 5.1: Performance comparison, averaged RMSE versus angular separation, with SNR = 32 dB and step size $\Delta\phi = 16$ (top) and $\Delta\phi = 32$ (bottom).

The results above show the fluctuation of the bias in the BF estimation, when varying the angular separation. We can also appreciate how the corrections applied, by using the LUT, reduce significantly the bias, containing the average RMSE within a range of [0.3°, 0.5°]. Actually, the pattern of fluctuation of the bias corresponds directly with the correction factors distribution, as it is shown in the figure below.

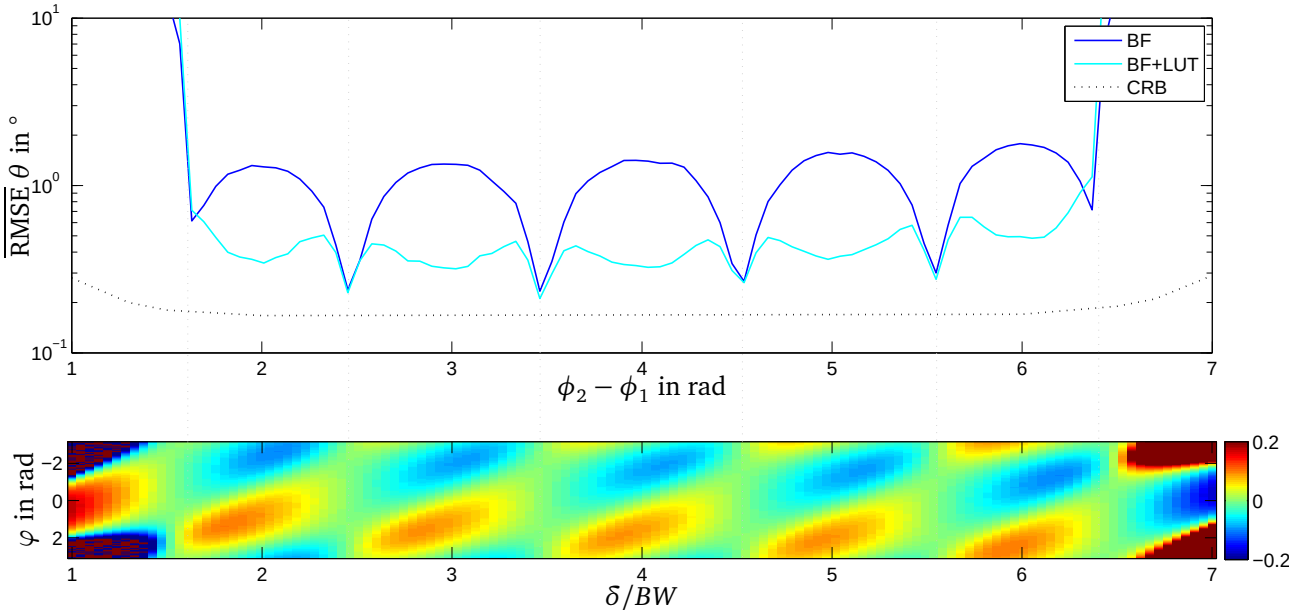

Figure 5.2: Bias of the BF estimates pattern: performance comparison, average RMSE versus angular separation (top), and correction factors distribution, corresponding to a 128-by-128 Lookup Table (bottom).

The performance of the BF using the LUT yields poor results for values of angular separation lower than $|\phi_2 - \phi_1|/BW \approx 1.6$. However, it is caused due to the BF spectrum evaluation at this area, which produce a single main beam, similar as it occurs in the non-resolved case. Therefore, this fact does not affect the performance of the proposed algorithm, because these situations will be solved as in non-resolved case by using high-resolution techniques, as it is described in the diagram proposed in Chapter 4.

Regarding the step size, we use the results showed in the Figure 5.1 to set the optimum value for each algorithm, attending to the compromise between accuracy and computational cost. Thereby, we consider a step size of $\frac{2\pi}{16}$ for the BF methods and $\frac{2\pi}{32}$ for the iterative algorithms.

A performance comparison, RMSE versus SNR, is shown in the Figure 5.3 (top). Since the behaviour of the BF method, using and not using the LUT, fluctuates along the angular separation, the results have been simulated by using random angular separations within the resolved case range. Thus, an averaged performance comparison is presented.

The computational cost is also given in the Figure 5.3 (bottom). The average CPU times are computed for the performance comparison simulation.

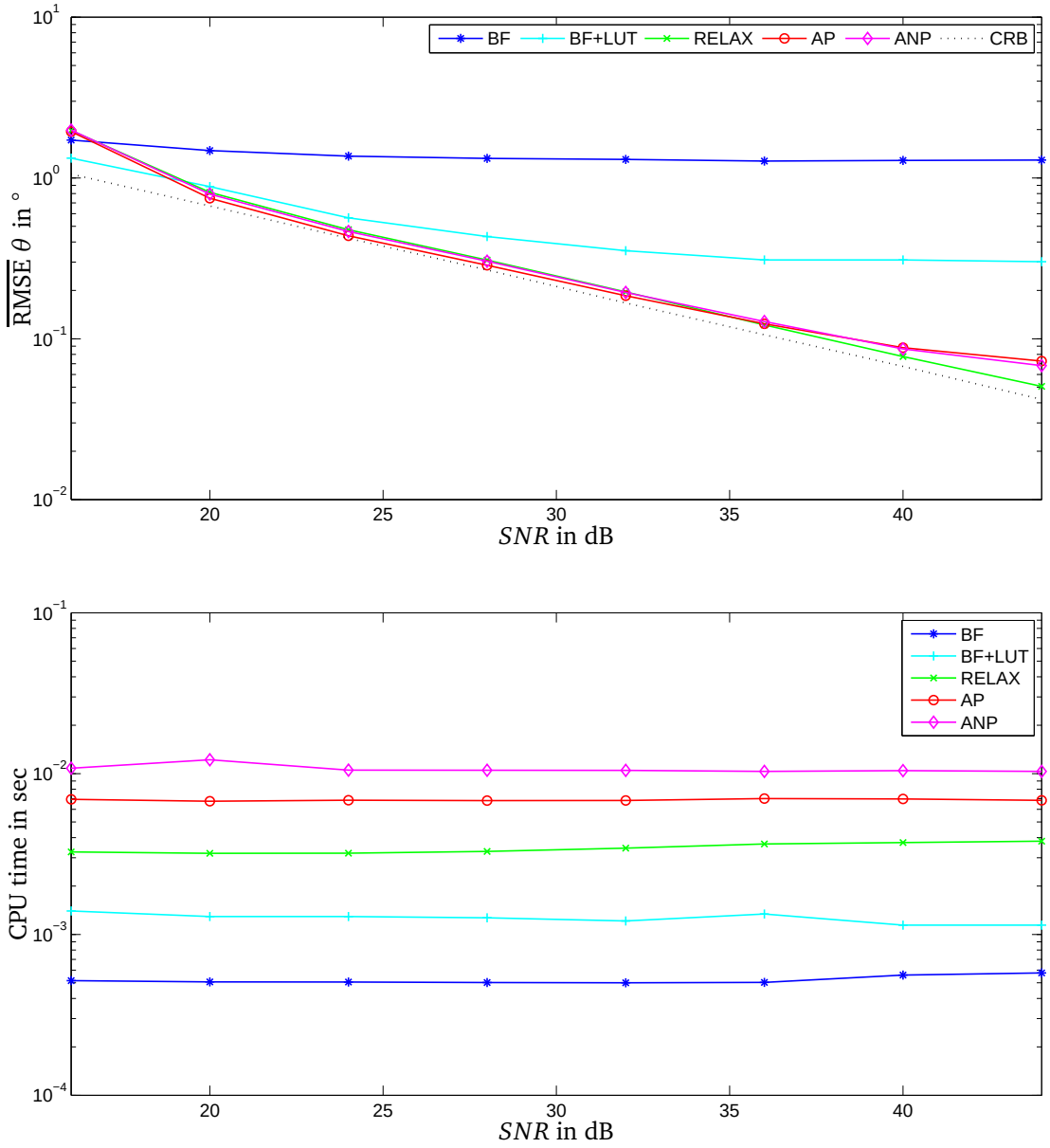

Figure 5.3: Performance comparison and computational cost comparison, with random angular separation within the resolved case range: averaged RMSE versus SNR (top) and CPU time versus SNR (bottom). The step size values are set to $\Delta\phi = \frac{2\pi}{32}$ (BF and BF+LUT) and $\Delta\phi = \frac{2\pi}{64}$ (RELAX, AP and ANP).

As it can be observed in the Figure above, the performance of the iterative algorithms is close to the CRB. Nevertheless, the computational cost is also expensive, mostly for the AP and ANP methods.

Despite being less close to the CRB, the BF technique using LUT corrections yields estimates with a converging error of 0.3°, which is acceptable for the automotive radar application [8]. Moreover, the estimation process requires only one-third of the time that the RELAX algorithm needs.

An extensive comparison between the BF method and the RELAX algorithm is given below. Figure 5.4 shows the averaged RMSE versus SNR (top), considering again random angular separations within the resolved case range. It is also shown the computational cost versus SNR (bottom).

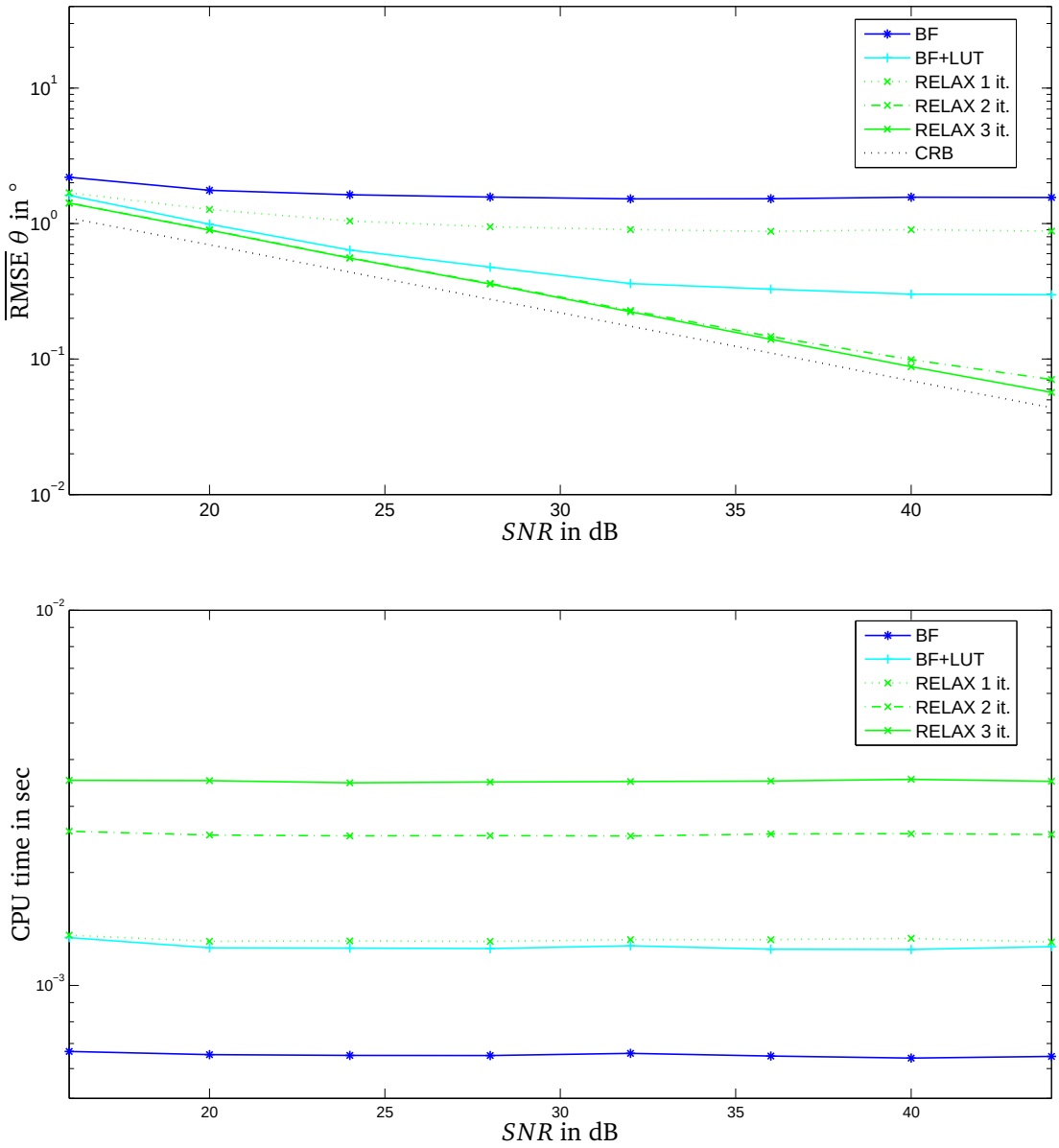

Figure 5.4: Comparison between the BF method and the RELAX algorithm, with random angular separation within the resolved case range: averaged RMSE versus SNR (top), and average CPU time versus SNR (bottom).

In the Figure above, the results of the RELAX algorithm are presented after 1, 2 and 3 iterations (green lines), in order to contrast the effectiveness of the "cleaning" process after each iteration. The BF method is simulated before and after applying the bias correction (blue and cyan lines, respectively).

It can be observed that the RELAX algorithm requires for one iteration almost as much time as the BF using correction factors, noting that the second method yields more accurate estimates.
After the second and the third iteration, the RELAX algorithm takes up two- and three-times the time required by the BF using the LUT, respectively.
Therefore, the proposed improvement for the BF method is shown as the fastest technique with an acceptable estimation error, considering angular separations within the resolved case range.

5.4.2 Non-resolved scenario

As in the resolved case, a performance comparison is first given. Figure 5.5 corresponds to the averaged RMSE versus angular separation, with $SNR = 32dB$.
We consider $\Delta\phi = \frac{2\pi}{96}$ for the Global Search technique, $\Delta\phi = \frac{2\pi}{32}$ for the RELAX algorithm and the AP method, and $\Delta\phi = \frac{2\pi}{96}$ for the ANP technique.

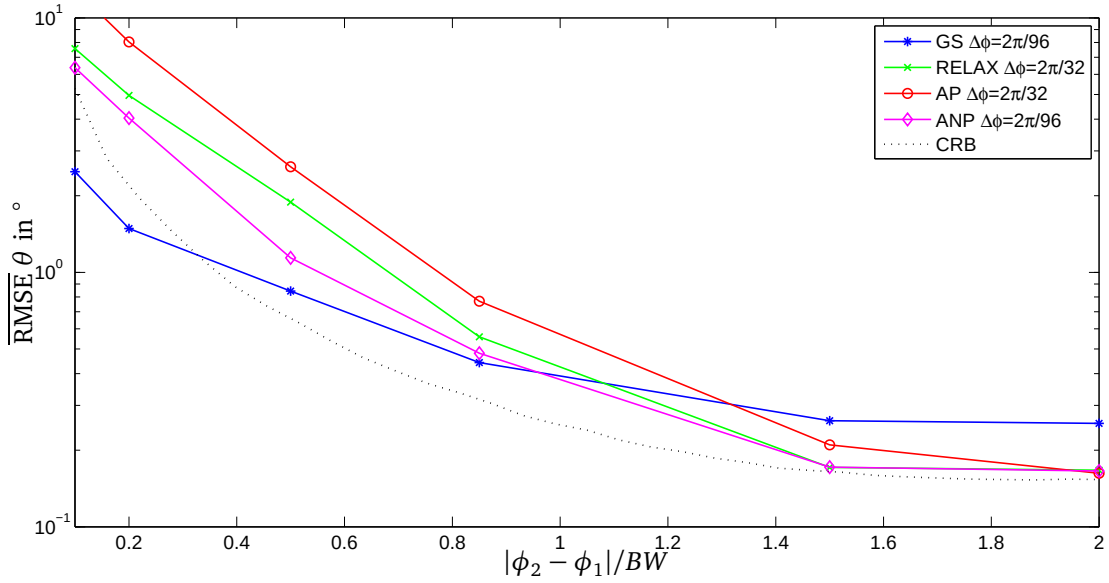

Figure 5.5: Performance comparison with SNR = 32 dB: averaged RMSE versus angular separation.

The first feature to note is the excellent result obtained by the Global Search for narrow angular separations, which is caused by delimiting the search range. This improvement adds information to the estimation process, thus reducing significantly the probability of great errors, and allowing results even below the CRB.
The Global Search performs better than the iterative algorithms, for values of angular separation $|\phi_2 - \phi_1| \gtrapprox BW$, which corresponds to the non-resolved case.

A final performance comparison is presented below. Figure 5.6 shows the averaged RMSE versus SNR, with angular separation $|\phi_2 - \phi_1| = 0.5BW$ (top) and $|\phi_2 - \phi_1| = 0.75BW$ (bottom). The step size is considered as described above. In the Figure 5.7 it is also shown the average CPU time versus SNR, which is computed for $|\phi_2 - \phi_1| = 0.75BW$.

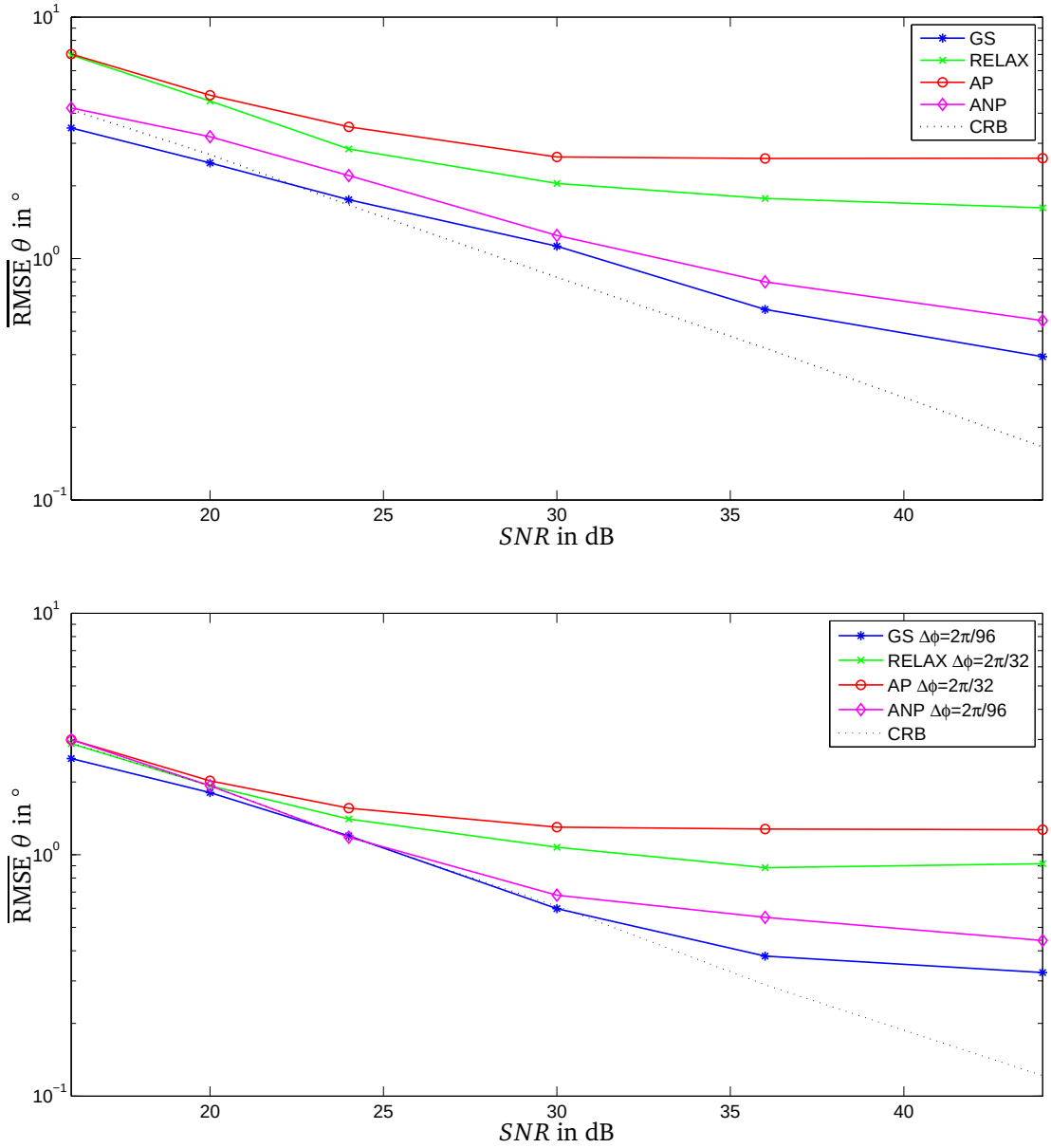

Figure 5.6: Performance comparison, averaged RMSE versus SNR, with angular separation $|\phi_2 - \phi_1| = 0.5BW$ (top) and $|\phi_2 - \phi_1| = 0.75BW$ (bottom).

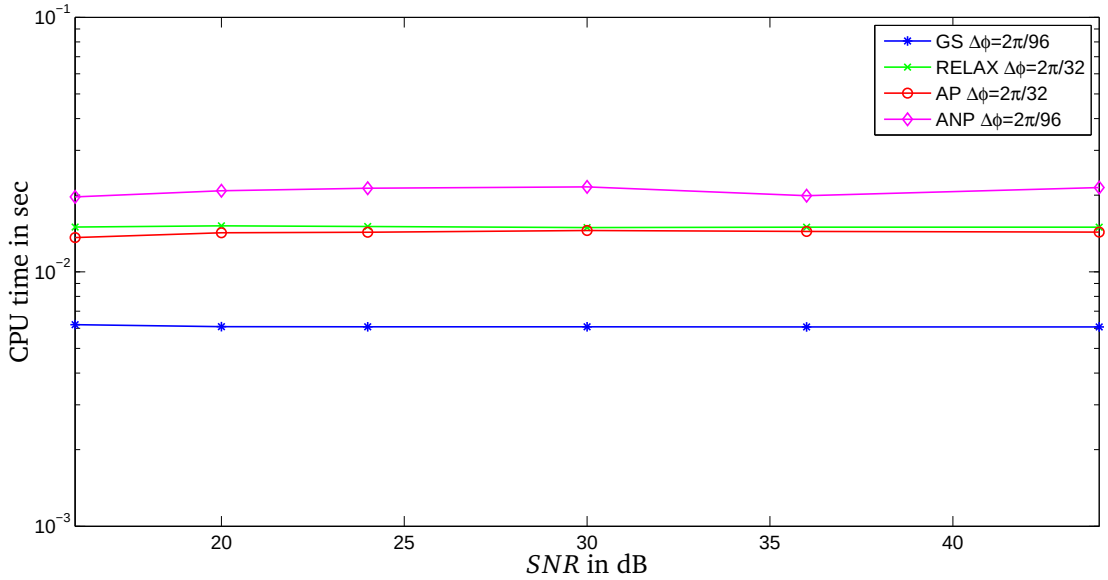

Figure 5.7: Computational cost comparison, CPU time versus SNR, with angular separation $|\phi_2 - \phi_1| = 0.75BW$.

As it can be observed in the Figure 5.6, the iterative algorithms yield quite biased estimates. Especially for the narrow angular separation, where the averaged RMSE is greater than 1°, also with good SNR.

The proposed Global Search technique is also biased, however, with a converging error of 0.4° for $|\phi_2 - \phi_1| = 0.5BW$, it is the unique algorithm to produce estimates which are accurate enough for the automotive radar application.
In spite of requiring a two-dimensional search, the simplifications applied allow a considerably reduction of the computational cost, which can be observed in Figure 5.7. Moreover, it has to be considered that the Global Search technique is not an iterative method, thus allowing also an easy parallelization by evaluating independently the cost function for each grid point.

6 Conclusion

In this thesis, we have considered the DOA estimation problem for two targets, focusing on the single-snapshot case. We have distinguished between the cases when the BF is able to resolve the two targets, and when it is not.
In the resolved scenario, the use of a look-up table has been proposed to reduce the bias of the BF estimates, which allows a fast implementation.
For the non-resolved scenario, we have considered the evaluation of the MLE cost function over a two-dimensional grid, in which an initial BF estimation is used to delimit the search range. Regarding the simplification of the cost function, the required projection operators can be calculated off-line in a simplified form and stored.
In order to further reduce the computational burden, a quadratic interpolation is used to obtain refined peak locations, which is applicable to estimate the global maximum from the BF spectrum as well as from the two-dimensional cost function evaluation.

The proposed methods have been compared with other MLE implementations. To be precise, we have considered the RELAX algorithm, the method of alternating projections and the ANP technique, all of them iterative algorithms. The resolved scenario has been simulated separately from the non-resolved case, evaluating first the RMSE versus the angular separation, for various step sizes, and second the RMSE versus SNR, showing also the corresponding computational time.

From the multiple simulations, the following results have been presented:

i) Resolved case:

- The LUT corrections considerably reduce the bias when estimating with the BF method.
- The converging RMSE of the proposed method is within the acceptable error range for the automotive radar application.
- The BF method using the LUT corrections requires only a third of the time of the fastest iterative algorithm.

ii) Non-resolved case:

- Comparing with the iterative algorithms mentioned, the Global Search is the unique algorithm to yield estimates which are accurate enough for the automotive radar application, with reasonable computational time.
- The improvements proposed considerably reduce the computational burden of the MLE cost function evaluation.
- The time required by the iterative algorithms is comparable to the resulted from the global search technique, however, this approach can be easily parallelized since it is not iterative.

We have also presented a block diagram which illustrates how to combine both methods, proposed as a suitable DOA estimation system for the automotive radar application.

Bibliography

[1] P. Heidenreich and A. M. Zoubir. Computational aspects of maximum likelihood DOA estimation of two targets with applications to automotive radar. *Proceedings of the 5th Biennial on DSP for In-Vehicle Systems, Kiel, Germany*, Sep 2011.

[2] J. Hwang and Y. Chen. Superresolution frequency estimation by alternating notch periodogram. *IEEE Trans. on Signal Processing*, 41(2):727–740, Feb 1993.

[3] H. Krim and M. Viberg. Two decades of array signal processing research. *IEEE Signal Processing Magazine*, 13(4):67–94, Jul 1996.

[4] J. Li and P. Stoica. Efficient mixed-spectrum estimation with applications to target feature extraction. *IEEE Trans. on Signal Processing*, 44:281–295, Feb 1996.

[5] D. Stenmanns P. Heidenreich and A. M. Zoubir. Computational simple criteria for detecting a multi-target scenario in automotive radar array processing. *Proceedings of the European Signal Processing Conference (EUSIPCO), Aalborg, Denmark*, Aug 2010.

[6] M. Richards. *Fundamentals of Radar Signal Processing*. McGraw-Hill, 2005.

[7] R. O. Schmidt. Multiple emitter location and signal parameter estimation. *IEEE Trans. Antennas Propagation*, pages 34(3):276–280, Mar 1986.

[8] M. Skolnik. *Introduction to Radar Systems*. McGraw-Hill, 2001.

[9] P. Stoica and A. Nehorai. Music, maximum likehood, and the cramér-rao bound. *IEEE Trans. Acoustics, Speech and Sig. Proc.*, pages 720–741, May 1989.

[10] H. Van Trees. *Detection, Estimation, and Modulation Theory - Part IV Optimum Array Processing*. Wiley and Sons, 2002.

[11] T. Tuncer and B. Friedlander. Classical and modern direction-of-arrival estimation. *Academic Press*, 2009.

[12] B.D. Van Veen and K.M. Buckley. Beamforming: A versatile approach to spatial filtering. *IEEE Signal Processing Magazine*, pages 4–24, Apr 1988.

[13] I. Ziskind and M. Wax. Maximum likelihood localization of multiple sources by alternating projection. *IEEE Trans. Acoustics, Speech and Signal Processing*, pages 36(10):1553–1560, Oct 1988.

[14] I. Ziskind and M. Wax. Maximum likelihood localization of diversely polarized sources by simulated annealing. *IEEE Trans. Antennas Propagation*, pages 38(7):1111–1114, Jul 1990.